Astronomy & Astrophysics manuscript no. output
March 31, 2025

Deciphering the Mass and Dynamics of Galaxy Pairs: The CenA/M83 and M81/M82 Groups

David Benisty[1], Noam Libeskind[1], and Yehuda Hoffman[2]

[1] Leibniz-Institut für Astrophysik Potsdam (AIP), An der Sternwarte 16, 14482 Potsdam, Germany

[2] Racah Institute of Physics, Hebrew University, Jerusalem 91904, Israel

ABSTRACT

This study extends the traditional Timing Argument (TA) - applied so far to the Local Group - to two nearby galaxy pairs, the Centaurus A-M83 complex and the M81-M82 pair. Given that only line-of-sight velocities are observable, assumptions must be made regarding the the internal dynamics of pairs of galaxies. As such, we employ two infall models: (i) Minor Infall, where the unmeasured velocity components are assumed to be zero, and (ii) Projected center of mass (CoM) model, that generalizes the Major Infall, where we assume both that the velocity of the CoM is purely along the line site and that the tangential velocity component is zero; namely the systems are radially infalling. For the M81-M82 system, both models agree on a radial infall velocity of approximately -300 km/s. When the TA is applied under these conditions, a mass estimate of $1.60^{+2.86}_{-1.07} \times 10^{12}\, M_\odot$ is returned, suggesting that these galaxies are on their first approach. In the CenA-M83 system, the minor infall model suggests a radial velocity of ~ 50 km/s, implying an unbound pair, while the Major Infall model predicts a bound system. The mass estimate of the CenA-M83 system for the unbound scenario is $3.45^{+2.65}_{-1.65} \times 10^{12}\, M_\odot$, and $1.48^{+0.68}_{-0.58} \times 10^{13}\, M_\odot$ for the bound case. The latter aligns well with the sum of the virial masses of the two galaxies of the CenA-M83 system, suggesting that the CenA-M83 are essentially infalling towards each other.

Key words. Galaxy pairs; Local Group; Cosmological Simulations; Redshift;

1. Introduction

The total mass of individual galaxies seems to be the most important parameter that determines the properties of a galaxy, yet the estimation of that mass is a formidable challenge Mo et al. (2010); Courteau et al. (2014). Nearby pairs of galaxies, that are close enough and yet do not strongly interacting are good candidates for such a study. The prime example of such a pair are the Milky Way (MW) and the Andromeda galaxies which together constitute the do-called Local Group (LG) Li & White (2008). Numerous methods and models have been applied to the LG aiming at the determination of its mass Peirani & de Freitas Pacheco (2006); Diaz et al. (2014); Peñarrubia et al. (2014); Wang et al. (2020). Of a particular interest is the *Timing Argument (TA)* model which treats the LG as an isolated two-body systems to estimate its mass. Here we attempt to apply the TA model to the nearby CenA/M83 and M81-M82 Groups.

By observing the current separation and velocities of galaxies like the MW and M31, one can work backward to estimate the time since their closest approach, often near the Big Bang. This inferred timescale, combined with gravitational dynamics, allows astronomers to calculate the system's total mass, including contributions from dark matter. The TA relates the mass of the LG to the kinematics of the MW-M31 system and the age of the universe.

The TA model treats the LG as an isolated classical two body system made of point-like particles of constant masses. The two particles are assumed to at zero separation at the onset of the Big Bang. Given the current distance and relative velocity of the MW-M31 pair and given the age of the Universe their total mass is readily evaluated. The TA assumes that the MW-M31 system is currently on its first approach in a two-body orbit, expanding after the Big Bang and now collapsing under mutual gravitational attraction. Early applications of TA assumed a purely radial orbit Li & White (2008); van der Marel et al. (2012), mostly due to the difficulty in measuring any proper motion. The TA were corrected with different effects. Subsequent refinements incorporated tangential motion van der Marel & Guhathakurta (2008), dark energy effects (Partridge et al. 2013; McLeod et al. 2017), modified gravity (Benisty & Capozziello 2023; McLeod & Lahav 2020), cosmic bias (van der Marel et al. 2012), and the MW's recoil velocity from the Large Magellanic Cloud (LMC) (Peñarrubia et al. 2016; Benisty et al. 2022; Benisty 2024; Chamberlain et al. 2023). These advances excluded the possibility of a past MW-M31 encounter (Benisty & Davis 2022) and extended the TA to model galaxy dynamics in local volume (Peñarrubia et al. 2014, 2016). Results have been compared to other mass estimation techniques, including numerical simulations (Li & White 2008; Lemos et al. 2021; Hartl & Strigari 2022, 2024; Sawala et al. 2023b,a; Wempe et al. 2024; Benisty et al. 2024).

Until now, the TA has been exclusively applied to the Local Group, mostly due to lack of good enough data. Yet there is no reason why such a calculation, could be applied beyond the local group. For the first time, we apply the TA to two galaxy pairs beyond the LG in the local Universe Karachentsev et al. (2002), focusing on the *Centaurus A/M83 (CenA-M83)* and *M81-M82* systems. The *CenA-M83 Group*, located about 5 Mpc away in the Centaurus constellation, is among the nearest galaxy groups to the LG and is crucial for studying galaxy formation and interactions Karachentsev (2005). CenA, an elliptical galaxy with an active nucleus, contrasts with M83, a spi-

ral galaxy known as the Southern Pinwheel. This group contains various types of dwarf galaxies, reflecting the variety found in galaxy clusters Jerjen et al. (2000). Prior studies of the CenA Group have examined its kinematics and dark matter distribution Jerjen et al. (2000), dark energy effects on its dynamics Teerikorpi et al. (2008), and local Hubble flow measurements Karachentsev et al. (2002, 2007). However, uncertainties in galaxy distances within the group remain a key challenge (Karachentsev et al. 2002). Additional work has explored CenA's dwarf satellites Müller et al. (2019) and the unexpectedly high number of dwarf galaxies in the M83 group, which poses challenges for ΛCDM cosmology Müller et al. (2021); Müller et al. (2024).

Unfortunately, just like the situation with M31 (until very recently), only line of sight peculiar velocities are measurable. Therefore assumptions have to be made regarding the dynamics and the unseen proper motion. Two assumptions have been been put forward in the literature by Karachentsev & Kashibadze (2006), known as the Minor and Major Infall model (see section IV). Such assumptions enables the application of the TA and thus an inferred mass to be calculated. By assuming infall between these galaxies, we estimate the total mass of the system and provide an upper limit on M83's tangential velocity around CenA. This marks a significant step toward applying the TA to galaxy groups beyond the LG.

This paper is organized as follows. Section (2) presents the predictions of the TA for galaxy pair masses in bound and unbound scenarios from different reference frames. Section (3) compares the TA model to simulations. Section (4) predicts the masses of the binaries and section (5) summarizes the results and gives predictions to improve the measurements.

2. Two Body Motion on the Sky

2.1. Timing Argument for bound and unbound systems

The Timing Argument is grounded in a mathematical framework that relies on several key assumptions. First, it considers an isolated system of two bodies, treating them as point masses with constant masses over time. The scenario begins at $t = 0$, corresponding to the Big Bang, with the two bodies initially separated by a small distance. The present time is defined as the age of the universe, t_U. These simplifying assumptions allow for the derivation of the dynamical evolution of the system, providing insights into the timing and motion of the two bodies within the context of cosmic expansion. The following derivation of the orbital dynamics of the gravitational two-body problem follows Will (2016). The dynamics of two bodies is governed by the energy per the reduced mass ϵ and the angular momentum l:

$$\epsilon = \frac{1}{2}\dot{r}^2 + \frac{l^2}{2r^2} - \frac{GM}{r}, \quad l = r^2\dot{\phi}, \tag{1}$$

where r is the separation, M is the total gravitating mass, G is Newton's constant and ϕ is the passage angle (or the true anomaly). In order to find the relation between the energy and the angular momentum to the eccentricity e and the semi-major axis a, we use the boundary condition that the time derivative of the separation is zero at the extremal separations (pericentre $a(1+e)$ and apocentre $a(1-e)$):

$$\dot{r}\left[a\left(1 \pm e\right)\right] = 0 \tag{2}$$

where e is the eccentricity and a is the semi-major axis. Inserting this condition into Eq. (1) yields the relations:

$$\epsilon = -\frac{GM}{2a}, \quad l^2 = GMa\left(1 - e^2\right), \tag{3}$$

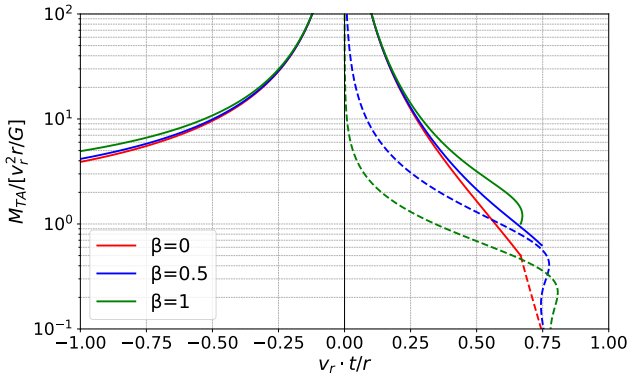

Fig. 1. *The inferred mass M_{TA} from the TA relations (Eqs. (9a) and (15)) given the observable $v_{rad} \cdot t/r$ and the ratio $\beta = v_{tan}/v_{rad}$. Negative (positive) values of $v_{rad} \cdot t/r$ correspond to approaching (receding) galaxy pairs. The smooth line presents the bound solution (ie $\epsilon < 0$) and the dashed presents the unbound solution ($\epsilon < 0$). For $v_{tan} = 0$ the bound and the unbound solutions give one unique solution for η. For higher tangential velocities there are few values for η for $v_{rad} > 0$.*

that connects the total energy and the angular momentum with the orbital parameters. We assume in this type of solution a bound solution with $\epsilon < 0$. In order to solve the two-body problem, it is useful to parameterize the separation as

$$r = a\left(1 - e\cos\eta\right). \tag{4}$$

where η is the eccentric anomaly Damour & Deruelle (1985) that defines the position of a body that is moving along an elliptic Kepler orbit. Inserting the parametrization (4) into Eq. (3) gives a differential equation for $\dot{\eta}$:

$$\frac{d\eta}{dt} = \sqrt{\frac{GM}{a^3}}\frac{1}{1 - e\cos\eta}. \tag{5}$$

The solution for this differential equation gives:

$$t = \frac{T}{2\pi}\left(\eta - e\sin\eta\right), \tag{6}$$

with the Kepler's 3rd law:

$$T = 2\pi\sqrt{\frac{a^3}{GM}}, \tag{7}$$

where T is the orbital period. Since we measure the velocities, we use the corresponding equations for the radial velocity $v_{\rm rad}$ and the tangential velocity $v_{\rm tan}$. The terms read:

$$v_{\rm rad} = \dot{r} = 2\pi\frac{a}{T}\frac{e\sin\eta}{1 - e\cos\eta}, \tag{8a}$$

$$v_{\rm tan} = \frac{l}{r} = 2\pi\frac{a}{T}\frac{\sqrt{1-e^2}}{1 - e\cos\eta}. \tag{8b}$$

For $t = 0$, the eccentric anomaly is also zero (Eq. 6) $\eta = 0$, and the minimum separation is given by: $r_{\rm min} = a(1-e)$, which reflects the TA implication that the separation was small at the beginning of the universe. For $v_{tan} = 0$, Eq. (8b) gives $e = 1$, namely a perfectly elliptical orbit.

The classical TA model assumes that at $t = 0$ the two bodies (i.e. galaxies) are at zero separation. This is inconsistent with

an elliptical orbit with a finite eccentricity. But the TA serves here as a simple toy model and t=0 is a proxy to an early time where the two-body system acquired its angular momentum and has settled into an elliptical orbit of a finite e. The extended TA model, which accommodates non-radial orbits, provides a theoretical framework for estimating the total mass of the system given the 3 observables - the distance of the pair of galaxies and their relative radial and tangential velocities - and an assumed age of the Universe. Given these the model enables the determination of the orbital parameters of the system, namely he eccentric anomaly (η) and the eccentricity:

$$\frac{v_{\rm rad}t}{r} = e\sin\eta\frac{\eta - e\sin\eta}{(1-e\cos\eta)^2} \tag{9a}$$

$$e = \frac{1}{\sqrt{1+\beta^2\sin^2\eta}}, \tag{9b}$$

where $\beta = v_{\rm tan}/v_{\rm rad}$. Inserting Eq. (8a) into Eq. (4) Solving Eqs. 9a and 9b to find η and e together with the Kepler's 3^{rd} law gives:

$$M_{\rm TA}^{\rm bound} = \frac{v_{\rm rad}^2 r}{G}\frac{1-e\cos\eta}{e^2\sin^2\eta}. \tag{10}$$

Fig (1) shows the relation of $v_{\rm rad}\cdot t/r$ and the predicted mass implied by the TA for various values of β. An upper bound on the mass exists for the case of $v_{tan} = \beta = 0$ and it is set by $v_{\rm rad}\, t/\, r = 2/3$, which is the maximal value of the right hand side of Eq. (9a). For larger values of v_{tan} we see a deviation for $v_{\rm rad} > 0$ from the $v_{tan} = 0$ case, but for the $v_{\rm rad} < 0$ the deviation is not large.

Since our focus is on binary galaxies outside the LG, we must also consider the possibility of unbound systems where $\epsilon > 0$. For such unbound cases, we must re-derive the equations of motion and thus we use the parametrization:

$$r = a\,(e\cosh\eta - 1)\,. \tag{11}$$

By generalizing the bound solution, we can modify the expressions for energy and angular momentum as follows:

$$\epsilon = \frac{GM}{2a}, \quad l^2 = GMa\left(e^2-1\right). \tag{12}$$

Using Eq. (1) along with the parametrization in Eq. (11), the temporal solution becomes:

$$t = \frac{T}{2\pi}\left(e\sinh\eta - \eta\right)\ . \tag{13}$$

The corresponding radial and tangential velocities are:

$$v_{\rm rad} = \dot{r} = 2\pi\frac{a}{T}\frac{e\sinh\eta}{e\cosh\eta - 1}\ , \tag{14a}$$

$$v_{\rm tan} = \frac{l}{r} = 2\pi\frac{a}{T}\frac{\sqrt{e^2-1}}{e\cosh\eta - 1}\ . \tag{14b}$$

For the unbound solution, the initial condition differs from the bound case. At $t = 0$, Eq. (13) yields $\eta = 0$. Substituting this into Eq. (11) gives the periapsis distance, $r_{\rm min} = a(e-1)$. To compute η, we consider the ratio $v_{\rm rad}t/r$, which provides the following relationship for η:

$$\frac{v_{\rm rad}t}{r} = e\sinh\eta\frac{e\sinh\eta - \eta}{(e\cosh\eta - 1)^2}. \tag{15}$$

The eccentricity, defined for $e > 1$, is expressed as:

$$e = \frac{1}{\sqrt{1-\beta^2\sinh^2\eta}}. \tag{16}$$

The TA mass derived from observables $v_{\rm rad}^2 r$ is given by:

$$M_{\rm TA}^{\rm unbound} = \frac{v_{\rm rad}^2 r}{G}\frac{e\cosh\eta - 1}{e^2\sinh^2\eta}. \tag{17}$$

Figure (1) illustrates the relationship between $v_{\rm rad}t/r$ and the TA mass. As Fig. (1) shows the behavior of the solutions varies depending on the value of $v_{\rm rad}t/r$. For values of $v_{\rm rad}t/r > 1$, there is no solution for the TA. In the range $0 < v_{\rm rad}t/r < 1$, both bound and unbound solutions exist, but they are not unique when $\beta > 0$. On the other hand, for $v_{\rm rad}t/r < 0$ a unique bound solution is observed. A special case arises when the tangential velocity $v_{\rm tan}$ is zero. In this scenario, the solutions converge smoothly at $v_{\rm rad}\cdot t/r = 2/3$, yielding continuous values. However, for larger values of $v_{\rm tan}$, the behavior changes, and the bound and unbound solutions become discontinuous. For specific values of $v_{\rm rad}\cdot t/r$, there may be no TA solutions or only a few isolated ones.

2.2. Local Group-like systems observed from the outside

The main objective, and novelty, of the paper is the application of the TA model to LG-like systems observed from outside the LG. Using the angular separation θ the physical distance r_{12} between the galaxy pair is determined by:

$$r_{12}^2 = r_1^2 + r_2^2 - 2r_1r_2\cos\theta, \tag{18}$$

where r_1 and r_2 are the distances of the galaxies from the observer. Fig (2) illustrates a pair of galaxies observed by an external observer, with line-of-sight velocities v_1 and v_2. The motion of galaxy 2 as seen by the galaxy 1 is decomposed into its the radial component $\boldsymbol{v}_{\rm rad}$ and the tangential one $\boldsymbol{v}_{\rm tan}$. Namely, the full relative motion between galaxy one and two reads:

$$\boldsymbol{v}_1 - \boldsymbol{v}_2 \equiv \boldsymbol{v}_{\rm rad} + \boldsymbol{v}_{\rm tan}. \tag{19}$$

The velocity vector can be written as a combination of three different components, the line-of-sight direction $\hat{r}^{\rm los}$, the perpendicular direction on the surface of the binary $\hat{r}^{\perp}$ and the observer and the direction perpendicular to the O12 plane defined by the observer and the 2 galaxies $\hat{r}^{\rm out}$:

$$\boldsymbol{v}_i = v_{i,\rm los}\hat{r}_i + v_{i,\perp}\hat{r}_{i,\perp} + v_{i,\perp}^{\rm out}\hat{r}_{i,\perp}^{\rm out}, \tag{20}$$

where $i = 1, 2$. We project Eq. (19) on $\hat{r}_1$ to get:

$$\begin{aligned} &v_{1,\rm los} - v_{2,\rm los}\cos\theta + v_{2,\perp}\sin\theta = \\ &v_{\rm rad}(\bar{r}_1 - \bar{r}_2\cos\theta) + \tilde{v}_{\rm tan}\bar{r}_2\sin\theta \end{aligned} \tag{21}$$

and on $\hat{r}_2$:

$$\begin{aligned} &v_{2,\rm los} - v_{1,\rm los}\cos\theta - v_{1,\perp}\sin\theta = \\ &v_{\rm rad}(\bar{r}_2 - \bar{r}_1\cos\theta) - \tilde{v}_{\rm tan}\bar{r}_1\sin\theta, \end{aligned} \tag{22}$$

where $\bar{r}_1 = r_1/r_{12}$, $\bar{r}_2 = r_2/r_{12}$ are the normalized distances and $\tilde{v}_{\rm tan} = v_{\rm tan}\sin i$ is projection of the tangential velocity on the O12. It is possible to isolate the radial velocity of galaxy 2 with respect to to the other one from these two equations to get:

$$v_{\rm rad} = \frac{v_{2,\rm los} - v_{1,\rm los}\cos\theta - v_{1,\perp}\sin\theta + \tilde{v}_{\rm tan}\bar{r}_2\sin\theta}{\bar{r}_2 - \bar{r}_1\cos\theta}, \tag{23}$$

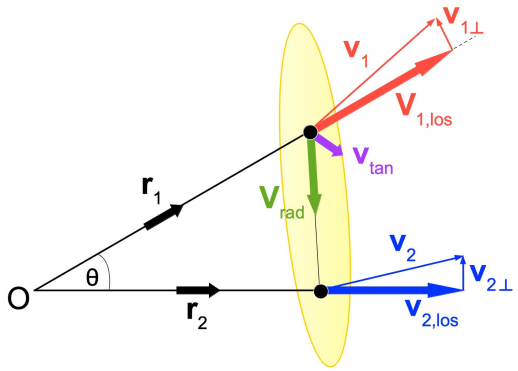

Fig. 2. *The relative motion of two galaxies, labeled as galaxy 1 and galaxy 2. The vector v_1 represents the velocity of galaxy 1, while v_2 represents the velocity of galaxy 2. The angle θ is measured between r_1 and the line connecting the two galaxies.*

and

$$v_{\rm rad} = \frac{v_{1,\rm los} - v_{2,\rm los}\cos\theta + v_{2,\perp}\sin\theta - \tilde{v}_{\rm tan}\bar{r}_1\sin\theta}{\bar{r}_1 - \bar{r}_2\cos\theta}. \quad (24)$$

For the case where one of the perpendicular velocities and the tangential velocities is zero, these Eq. are useful to determine the radial velocity. For $v_{1,\perp} = v_{\rm tan} = 0$, the model is often called the Major Infall Model Karachentsev & Nasonova (2010); Wagner & Benisty (2025). For $v_{1,\perp} = v_{\rm tan} = 0$ is the Major infall from the projection on galaxy two, and $v_{2,\perp} = v_{\rm tan} = 0$ is the Major infall projected from galaxy one. These two options are not symmetric.

The projection is done on one of the galaxies and the assumption is that the perpendicular motion and tangential velocity of the other galaxy is small. From these two equations we solve the radial and the projected tangential velocities:

$$\begin{aligned} v_{\rm rad} &= v_{1,\rm los}\bar{r}_1 + v_{2,\rm los}\bar{r}_2 - \cos\theta\left(v_{1,\rm los}\bar{r}_2 + v_{2,\rm los}\bar{r}_1\right) \\ &\quad + \sin\theta\left(v_{2,\perp}\bar{r}_1 - v_{1,\perp}\bar{r}_2\right), \end{aligned} \quad (25)$$

and for $\tilde{v}_{\rm tan} \equiv v_{\rm tan}\sin i$:

$$\begin{aligned} \tilde{v}_{\rm tan} &= v_{1,\perp}\bar{r}_1 + v_{2,\perp}\bar{r}_2 - \cos\theta\left(v_{1,\perp}\bar{r}_2 + v_{2,\perp}\bar{r}_1\right) \\ &\quad + \sin\theta\left(v_{2,\rm los}\bar{r}_1 - v_{2,\rm los}\bar{r}_2\right). \end{aligned} \quad (26)$$

The unknown are $v_{2,\perp}, v_{1,\perp}$. The assumption that the perpendicular velocities are small $v_{2,\perp} = v_{1,\perp} = 0$, is often called the **Minor Infall Model**. This is essentially a minimal model where only the actual observed line-of-sight velocities are considered and the other components are assumed to be negligible - it follows that $v_{\rm tan}$ is negligible as well. In this case $v_{\rm rad}$ can be written:

$$v_{\rm rad} = v_{1,\rm los}\bar{r}_1 + v_{2,\rm los}\bar{r}_2 - \cos\theta\left(v_{1,\rm los}\bar{r}_2 + v_{2,\rm los}\bar{r}_1\right). \quad (27)$$

We suggest a new model form of the infall velocity, where both galaxies are moving towards the CoM. In this reference frame we can assume that:

$$\boldsymbol{v}_{\rm c} = v_{\rm c}\hat{r}_c, \quad \boldsymbol{v}_{\rm c,\perp} = 0, \quad (28)$$

where $\boldsymbol{v}_{\rm c}$ is the line of sight CoM velocity The CoM position and velocity of the pair read:

$$\boldsymbol{r}_c = \bar{m}_1\boldsymbol{r}_1 + \bar{m}_2\boldsymbol{r}_2, \quad \boldsymbol{v}_c = \bar{m}_1\boldsymbol{v}_1 + \bar{m}_2\boldsymbol{v}_2, \quad (29)$$

where the normalized masses are: $\bar{m}_1 = \frac{m_1}{m_1+m_2}$ and $\bar{m}_2 = \frac{m_2}{m_1+m_2} \equiv 1 - \bar{m}_1$. The radial velocity between the galaxies $v_{\rm rad}$ can be expressed from the CoM with the components: $\bar{m}_2 v_{\rm rad}$ and $-\bar{m}_1 v_{\rm rad}$.

Model	What is zero?	Final Equation term
Minor	$v_{1,\perp}, v_{2,\perp}$	Eq. (27)
Major on galaxy 1	$v_{2,\perp}, v_{\rm tan}$	Eq. (23)
Major on galaxy 2	$v_{1,\perp}, v_{\rm tan}$	Eq. (24)
Projected CoM	$v_{c,\perp}, v_{\rm tan}$	Eq. (32)

Table 1. *The assumptions for different infall models. For any model the table shows the assumption that sets some of the velocity components to zero and gives ref to the final Eq. for the infall model. To estimate the TA masses we use the* ***Minor Infall*** *and the* ***Projected CoM*** *models.*

Therefore, the velocity vectors from the center are expressed via:

$$v_c\hat{r}_c + \bar{m}_2 v_{\rm rad}\hat{r}_{21} = \boldsymbol{v}_1, \quad v_c\hat{r}_c - \bar{m}_1 v_{\rm rad}\hat{r}_{21} = \boldsymbol{v}_2. \quad (30)$$

We project these two equations on $\hat{r}_1$ and $\hat{r}_2$ give the scalar equations:

$$\begin{aligned} v_c\left(\bar{m}_1\bar{r}_1 + \bar{m}_2\bar{r}_2\cos\theta\right) + \bar{m}_2 v_{\rm rad}\left(\bar{r}_2\cos\theta - \bar{r}_1\right) &= v_{1,\rm los}, \\ v_c\left(\bar{m}_1\bar{r}_1\cos\theta + \bar{m}_2\bar{r}_2\right) - \bar{m}_1 v_{\rm rad}\left(\bar{r}_2 - \bar{r}_1\cos\theta\right) &= v_{2,\rm los}, \end{aligned} \quad (31)$$

where we use the identities from the appendix. The solution for these two equations give the radial infall solution:

$$v_{\rm rad} = \frac{\bar{m}_1\bar{r}_1 v_{2,\rm los} - \bar{m}_2\bar{r}_2 v_{1,\rm los} - \cos\theta\left(\bar{m}_1\bar{r}_1 v_{1,\rm los} - \bar{m}_2\bar{r}_2 v_{2,\rm los}\right)}{\bar{r}_1\bar{r}_2\Delta\bar{m} + \cos\theta\left(\bar{m}_1\bar{r}_1^2 - \bar{m}_2\bar{r}_2^2\right)}. \quad (32)$$

where $\Delta\bar{m} = \bar{m}_1 - \bar{m}_2$. We call this model the **Projection CoM** model. For $\bar{m}_1 = 1$ we get the Major Infall projected on galaxy one, and for $\bar{m}_2 = 1$ we get the projected on galaxy two. The advantage of this projection is the lack of the dependence of the $v_\perp$.

Table 1 summarizes the different infall models and their assumptions. The Projected CoM model uses the unknown ratio of the two masses, hence the application of the model needs to employ a prior assumption on the probability of that ratio. This addressed in Sec. 3.

3. Timing Argument Validation by Simulation

The various versions of the TA model are tested here against the publicly available *AbacusSummit Simulation* suite Maksimova et al. (2021). This suite is particularly well suited because it includes a high-resolution run, with particle masses of $m_{\rm part} = 2\times10^9\,h^{-1}M_\odot$, within a large simulation box of size $L_{\rm box} = 2$ Gpc/h. The simulations were conducted on a range of cosmological models; here, we use the fiducial Planck 2018 cosmology Aghanim et al. (2020). This setup produces a robust halo catalog, containing approximately 12×10^6 halos with masses greater than $10^{11}\ M_\odot$ (i.e., a 100-particle limit).

The analysis is based on the $z = 0$ halo catalog, constructed using a spherical overdensity algorithm applied after an initial friends-of-friends grouping of dark-matter particles Maksimova et al. (2021). The catalog includes halos with masses in the range, enabling a comprehensive sample of isolated galaxy pairs analogous to the M81-M82 and Cen A-M83 systems. The pair-finding algorithm proceeds as follows:

– Halos with masses between $5\cdot10^{11} \le M_{\rm halo} \le 5\cdot10^{13}\,M_\odot$ are selected for analysis.

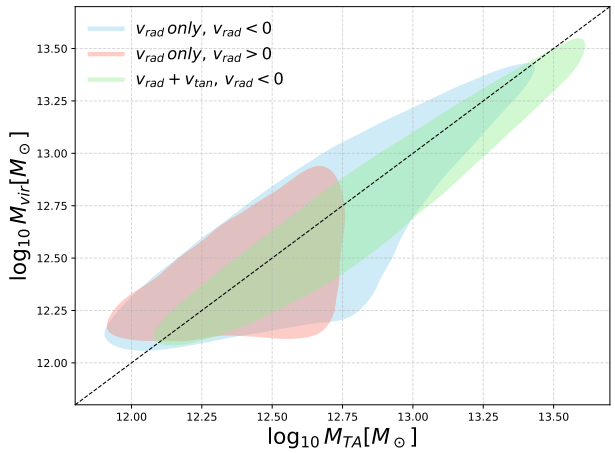

Fig. 3. *Dependence of tangential velocity on the TA predictions for systems with $v_{tan}/|v_{rad}| < 3$. The radial TA model (using only V_{rad} exhibits slightly larger scatter than the full TA model (including $V_{rad}+V_{tan}$, while the unbound case shows the highest scatter.*

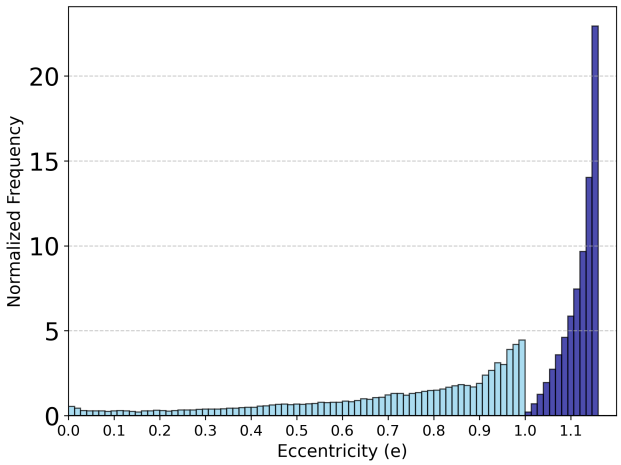

Fig. 4. The eccentricity distribution from the isolated pairs in the simulations for the bounded (cyan) and the unbounded (blue) cases. The distribution of the eccentricities of the bounded pairs is skewed towards the radial orbits.

- Each halo in this range is paired with a *single* neighboring halo that meets the following criteria: (1.) The partner must have a greater mass than the original halo. (2.) The partner must be within a 3D distance of 2 Mpc. (3.) No other halos with $M_{\rm halo} \geq 10^{11}\,M_\odot$ can exist within a radius smaller than the distance to the selected partner.
- Each halo can participate in at most one pair, ensuring no duplication or overlap.
- The relative radial velocity between paired halos must be less than 100 km/s.

This approach captures diverse galaxy pair configurations while enforcing isolation, mass hierarchy, and dynamical coherence, critical for studying systems akin to observed interacting pairs.

The TA model estimates halo masses using dynamical orbital constraints. The radial TA considers only radial velocity ($V_{\rm rad}$), while the full TA incorporates both radial and tangential motions ($V_{\rm rad} + V_{\rm tan}$). The unbound case refers to particles exceeding the system's gravitational binding criteria, leading to larger scatter in mass estimates.

Fig. (3) shows the correlation between the total halo masses of the binary galaxies and the predicted TA mass. With a cut-off of $v_{\rm tan}/|v_{\rm rad}| < 3$, most pairs are close to the straight line of the one-to-one correlation. For larger $v_{\rm tan}/|v_{\rm rad}|$, the pairs deviate from the one-to-one line, implying that the TA gives the best predictions for low $v_{\rm tan}$. Including $v_{\rm tan}$ (full TA) provides a slightly tighter estimate for the virial mass compared to the radial TA, which ignores tangential motion. However, since for observed galaxy pairs we can only directly estimate the radial velocity (and the projected $v_{\rm tan}$ on the sky), we adopt the radial TA with its statistical scatter to estimate the total mass of the pair.

Fig. (4) shows the inferred eccentricity distribution from the isolated pairs in the simulations for the bounded and unbounded cases. The majority of bound pairs are in direct radial infall ($e = 1$), justifying the radial TA as a reasonable approximation. The scatter in virial mass estimates, particularly for the unbound case, reflects deviations from purely radial orbits and underscores the limitations of the TA framework in systems with significant tangential motion.

The decision to avoid using the tangential velocity (v_t) directly from measurements stems from its dependence on $\sin i$, as shown in Eq. (26), where the inferred quantity becomes $v_t \propto 1/\sin i$. This introduces a divergence as $\sin i \to 0$ (edge-on orbital configurations), leading to unconstrained v_t values, especially under the uniform prior $\sin i \in [-1, 1]$. To resolve this, the eccentricity is related to the projected angle via: $e \sim |\sin i|$ (from Eq. 9b) which incorporates $\sin i$ alongside geometric terms ($\sin\theta$, $\sin\eta$). e is constrained to $[-1, 1]$ ensuring that even as $\sin i \to 0$, the eccentricity remains finite and physical, peaking near $e \approx 0$ nearly circular orbits. However, the system's mass, inferred from Eqs. (10) and (17) scales inversely with e as $M \sim 1/e$. Small $\sin i$ values (approaching edge-on inclinations) suppress e, inflating the inferred mass to poorly constrained levels. This degeneracy between $\sin i$ and M introduces significant bias, particularly in low-inclination systems. To circumvent this, the analysis prioritizes the radial TA model, which avoids direct dependence on $\sin i$, and instead corrects for scatter using simulations.

4. Mass Determination

4.1. Data and Relative Motion

The two TA models of Sec. 2.2 are applied here to the two nearest LG-like systems: Centaurus A - M83 and the M81-M82 pair. The CosmicFlows 4 dataset (Tully et al. 2023, CF4) of galaxy distances is used here to infer the distances and line-of-sight velocities of the 4 galaxies of these binary systems.

The TA mass of the two systems is assessed here by performing Monte Carlo realizations of the uncertainties in the distances and the radial velocities as given by the CF4 database. The errors on the distance moduli are assumed to be normally distributed, which implies that the uncertainties on the inferred distances and velocities are lognormal distributed. The application of the Projected COM model requires an assumption on the unknown mass ratio of m_1 and m_2. Here we assume a uniform prior on the galaxy mass ratio $\in [0, 1]$. Fig. (5) illustrates the distribution of inferred distances and infall velocities derived from the data in Table 2, with the corresponding values presented in Table 3.

For the M81-M82 system, the values from both models are approximately -300 km/s, suggesting a very small angle and minimal contributions from both tangential and perpendicular components. In contrast, for the CenA-M83 system, our analysis reveals a strikingly narrow range for the radial velocity: $-50 < v_{\rm rad} < 50$ km/s. This result—whether interpreted as mod-

Galaxy	PGC	RA [^{O}]	Dec [^{O}]	D [Mpc]	cz [km/s]	Ref.
CenA	46957	204.254	-29.866	3.63 ± 0.06	547 ± 5	Hunt et al. (2021); Paturel et al. (1999)
M83	48082	201.365	-43.019	4.83 ± 0.09	513 ± 2	Díaz et al. (2006); Allison et al. (2014)
M81	28630	148.888	69.065	3.62 ± 0.21	−39 ± 3	Truebenbach & Darling (2017); Speights & Westpfahl (2012)
M82	28655	148.968	69.680	3.53 ± 0.03	269 ± 2	Gendre et al. (2013); van der Tak et al. (2008)

Table 2. *The distances and heliocentric velocities from CF4 Tully et al. (2023).*

System	r [Mpc]	$v_{\mathrm{rad,min}}$ $[km/s]$	$v_{\mathrm{rad,com}}$ $[km/s]$
CenA - M83	1.51 ± 0.08	$54.4^{+6.64}_{-6.28}$	$-47.9^{+17.2}_{-16.6}$
M81 - M82	$0.15^{+0.16}_{-0.09}$	$-297.58^{+6.59}_{-8.18}$	$-318.52^{+4.57}_{-6.04}$

Table 3. *The inferred relative quantities of different galaxy pairs and the corresponding TA mass using the two infall velocity models. For a comparison, we include the measured distances and the radial velocity of M31 from us and its TA mass.*

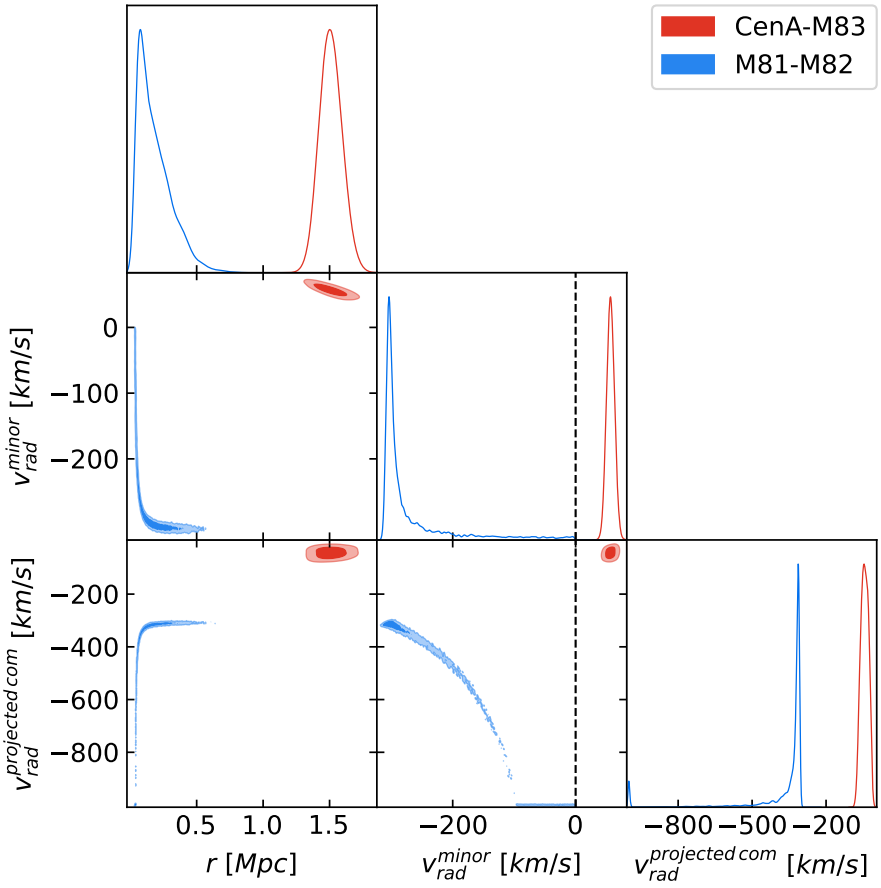

Fig. 5. *Probability distribution functions (diagonal plots) and probability density contours (off-diagonal plots) for predicted separation and radial velocities based on two different models. For the M81-M82 system, both models yield similar predictions. However, for the CenA-M83 system, the projected-com infall model predicts radial infall, whereas the other model predicts radial runaway.*

est infall (∼ −50 km/s) in the projected CoM case or a mild positive velocity (∼ 50 km/s) in the minor infall model indicates that the mutual gravitational influence between CenA and M83 is exceptionally weak.

While observational uncertainties in radial velocities leave ambiguity about the system's exact dynamical state, our models robustly constrain v_{rad} to a remarkably small magnitude. This implies that CenA and M83 are either loosely bound with negligible ongoing interaction or following minimally perturbed trajectories. Such a low-velocity regime aligns with scenarios where the galaxies are only weakly affecting one another, whether temporarily coincident in their orbits or evolving largely independently. Despite Ref. Karachentsev et al. (2007) argues for an unbound configuration, our work presents the first evidence for a possible bound infall scenario between CenA and M83.

4.2. TA mass

The mass distributions inferred from the extended timing infall model for both galactic systems are displayed in Fig. (7) in dashed lines, where the solid lines are with the correction from simulations. Since the radial velocities for M81-M82 system are compatible with each other the TA masses are very close to each other, which is around, with average value of $2.28^{+2.64}_{-1.98} \times 10^{12} \times M_{\odot}$. However for the Cen A-M83 complex the masses are different from each other: while for the minor

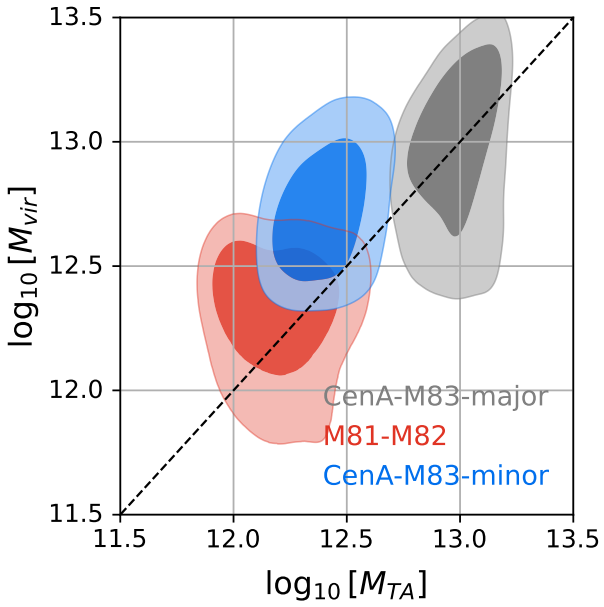

System	Range	$M_{\rm vir}/M_{\rm TA}$
CenA - M83 [Minor]	$r \in [1.2, 1.8]$ Mpc $v_{\rm rad} \in [0, 70]$ km/s	$2.17^{+1.14}_{-0.83}$
CenA - M83 [P. CoM]	$r \in [1.2, 1.8]$ Mpc $v_{\rm rad} \in [-80, 0]$ km/s	$1.31^{+0.54}_{-0.51}$
M81 - M82 (Minor and P. CoM)	$r \in [0., 0.5]$ Mpc $v_{\rm rad} \in [-350, -250]$ km/s	$0.71^{+0.62}_{-0.34}$

Fig. 6. *The correlation between the predicted TA mass, M_{TA}, and the total virial mass of the halos, M_{Vir}, for galaxy pairs. The top panel represents CenA-M83-like pairs, while the bottom panel represents M81-M82-like pairs. The table below show the prior range for the Minor Infall model and for the Projected CoM model, and the $P(M_{vir}/M_{TA})$ distribution value.*

infall, the model predicts a unbound radial "run away" and the TA gives a mass of $1.50 \pm 0.69 \times 10^{12}\,M_\odot$, the projected CoM model gives a radial infall bound motion with larger mass of $11.43 \pm 1.43 \times 10^{12}\,M_\odot$. This inconsistency shows that there is at least one projected velocity that we are not able to measure directly, as expected from our assumptions.

4.3. Mass Inference from Simulations

Fig. (6) shows the correlation between the TA mass and the virial mass from simulations for pairs with radial infall or radial run-away. For radiali bound systems, the TA predicts better the total mass of the pair. To address the simulated pairs, simulation have traditionally been used to estimate the typical corrections which account for these biases and provide more accurate mass predictions. Given the observables one would like to infer the true mass from simulations, where the simulated mass here is M_{sim}. Hence,

$$P(M_{\rm sim}|M_{\rm TA}, \xi) = \int P(M_{\rm TA}|\xi, M_{\rm sim}) P(M_{\rm sim}|\xi) d\xi, \quad (33)$$

where $\xi = r, v_{\rm rad}$ represents the key observables. This approach integrates over the parameter space of ξ, linking the simulated masses ($M_{\rm sim}$) to the corrected TA masses. Here, $P(M|\xi, M_{\rm sim})$ denotes the likelihood of obtaining a TA mass M, given the observables ξ and simulated mass $M_{\rm sim}$. The prior term $P(\xi|M_{\rm sim})$ represents the expected distribution of observables in simulations for a given $M_{\rm sim}$.

Fig. (6) illustrates the correlation between the predicted TA mass and the total virial mass of the halos for galaxy pairs assuming different models. After applying corrections to TA masses, the predicted values for the M81-M82 are averaged to $1.60^{+2.86}_{-1.07}\,10^{12}\,M_\odot$. For Cen A-M83 the values are $3.45^{+2.65}_{-1.65} \times 10^{12}\,M_\odot$ for the minor unbound model and $14.83^{+6.68}_{-5.81} \times 10^{12}\,M_\odot$ for the Projected CoM bound model.

4.4. Other Mass Estimates

We compare the masses of galaxy systems using independent estimates derived from various methodologies. The Cen A–M83 galaxy system has been extensively studied, with mass estimates showing significant variation depending on the method employed. The orbital and virial mass estimates place the Cen A group in the range of $(6.4 - 8.1) \times 10^{12}\,M_\odot$, while the M83 group is found to have a smaller orbital or virial mass of $(0.8 - 0.9) \times 10^{12}\,M_\odot$. The total mass of the combined system is reported as $(6.0 \pm 1.4) \times 10^{12}\,M_\odot$ Karachentsev et al. (2007). Later estimations with the MUSE observations get $2.5^{+0.7}_{-0.6} \times 10^{12}\,M_\odot$ "Müller et al. ("2024"), which yields $8.9^{+1.89}_{-1.94} \times 10^{12}\,M_\odot$ for the total system.

In contrast, studies based on the Hubble flow fit provide significantly smaller mass estimates for the Cen A–M83 system. For instance, Peirani & Pacheco (2008) reports a total mass of $(2.1 \pm 0.5) \times 10^{12}\,M_\odot$, and Del Popolo & Chan (2022) finds a comparable value of $(2.81 \pm 0.50) \times 10^{12}\,M_\odot$. These results are systematically lower than those derived from the virial theorem. This discrepancy can be attributed to the different assumptions underlying these methods. The virial theorem assumes that the system is dynamically relaxed and fully bound, which may overestimate the mass if there are unbound or outlying components. In contrast, the Hubble flow fit is sensitive to the large-scale dynamics and may underestimate the mass if the system is not entirely gravitationally bound, or if systematic errors affect distance estimates.

A similar analysis applies to the M81–M82 galaxy system, where mass estimates also vary across different methodologies. Virial mass estimates for this system place the total mass within a range of $(1.03 \pm 0.17) \times 10^{12}\,M_\odot$ to $(1.29 \pm 0.14) \times 10^{12}\,M_\odot$ Karachentsev & Kashibadze (2005), with an earlier study reporting $(1.6 \pm 0.3) \times 10^{12}\,M_\odot$ Karachentsev, I. D. et al. (2002). The total mass within the turnaround surface, derived from the virial theorem, is found to be $1.2 \times 10^{12}\,M_\odot$. However, estimates based on the Hubble flow fit are generally smaller. For example, Peirani & Pacheco (2008) reports $(0.92 \pm 0.24) \times 10^{12}\,M_\odot$, while Del Popolo & Chan (2022) finds $(1.40 \pm 0.10) \times 10^{12}\,M_\odot$.

As with the Cen A–M83 system, the Hubble flow estimates for the M81–M82 system tend to yield lower values than those derived from the virial theorem. The discrepancy is less pronounced in this case, but it still reflects the inherent differences between the two methodologies. The virial theorem-based estimates are likely to capture the mass of gravitationally bound components more effectively, while the Hubble flow estimates are influenced by larger-scale dynamics, which may lead to underestimations if some portions of the system are not fully bound.

As shown in Fig. (7) the comparison of mass estimates for the Cen A–M83 and M81–M82 systems reveals systematic differences between the methodologies employed. For Cen

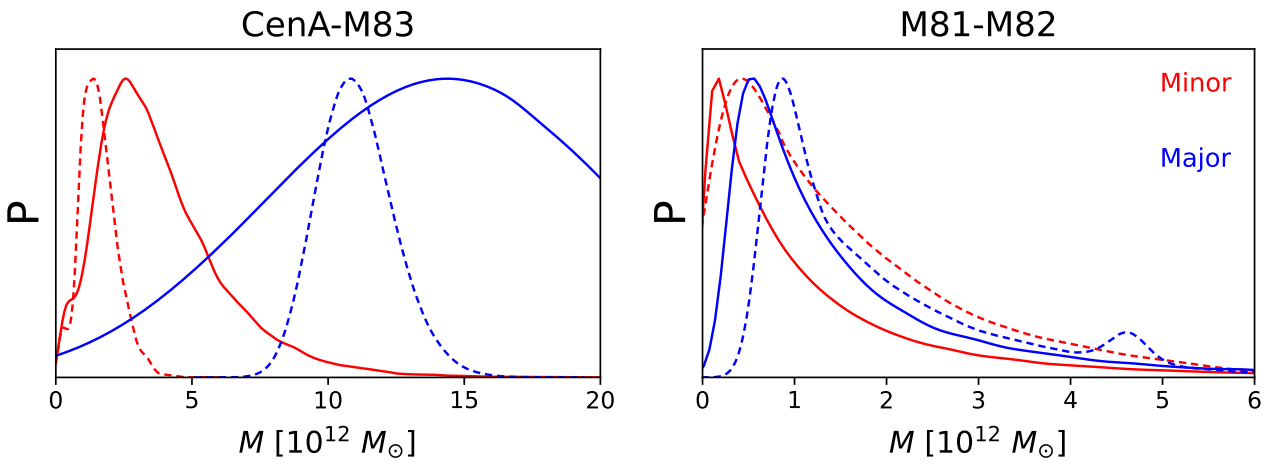

System	$M_{\rm TA,\ minor}$ [$10^{12}\,M_\odot$]	$M_{\rm TA,\ CoM\ major}$ [$10^{12}\,M_\odot$]	$M_{\rm TA,\ minor,\ sim}$ [$10^{12}\,M_\odot$]	$M_{\rm TA,\ CoM\ major\ +\ sim}$ [$10^{12}\,M_\odot$]
CenA - M83	1.50 ± 0.69	$3.45^{+2.65}_{-1.65}$	11.43 ± 1.43	$14.83^{+6.68}_{-5.83}$
M81 - M82	2.61 ± 2.31	$1.90^{+2.88}_{-1.08}$	2.59 ± 1.98	$1.30^{+2.87}_{-1.06}$

Fig. 7. *The posterior distribution for the galaxy pairs studies in this research for the pure TA (dashed lines) vs. the TA corrected by the spread from simulations (smooth line). The minor and the major based estimates gives closer values for the masses due to the tiny 2D projected angle on sky. The large bias between the major and the minor based masses implies for additional velocity component that we don't directly measure.*

A–M83, given the virial mass we can select the better estimation for the radial motion between the galaxies. Our selection predicts the radial infall and matching with completely independent method for the mass estimate. In contrast, for the M81–M82 system, all methods converge more closely, indicating greater agreement between the virial mass and Hubble flow estimates. These findings underscore the variability in mass estimations depending on the method used and highlight the importance of cross-validation in galaxy system analyses.

5. Discussion

This research examines, for the first time, the mass estimates of the Cen A–M83 and M81–M82 galaxy systems using theTA. This approach refines the methodology for reconciling observational constraints with the cosmological dynamics of galaxy pairs modeled as binary systems. A key challenge in applying the TA to galaxy pairs on the sky is determining their radial velocities. While the radial velocity of M31 relative to the Milky Way (MW) is directly measurable via redshift, this is not feasible for arbitrary galaxy pairs. To address this, we employ two distinct models—the **Minor Infall** and **Projected CoM Infall** models—to infer radial velocities and predict system masses using TA combined with simulation-based inference.

For the Cen A-M83 system, the separation distribution peaks at $\sim$ 1.5 Mpc, with inferred infall velocities varying between models. The Minor Infall model suggests velocities of $\sim$ 50 km/s, whereas the Projected CoM model indicates faster infall at ~ -50 km/s. The M81–M82 system shows greater uncertainty in separation, peaking at $\sim$ 0.1 Mpc with a radial infall velocity of approximately -300 km/s.

The Local Group (LG), comprising the MW and M31, has been a benchmark for TA-based mass estimates. Prior studies report a separation of 0.77 ± 0.04 Mpc and a radial velocity $v_{\rm rad} = 109.3 \pm 4.4$ km/s for the MW–M31 system, yielding a TA-derived mass of $4.17 \pm 0.44) \times 10^{12} M_\odot$ van der Marel & Guhathakurta (2008); van der Marel et al. (2012). However, simulations incorporating tidal interactions and LG membership suggest a lower virial mass, with a correction factor $M_{\rm vir}/M_{\rm TA} = 0.70^{+0.21}_{-0.17}$. Applying this factor gives a revised mass of $2.92 \pm 0.77) \times 10^{12} M_\odot$, consistent with independent estimates from satellite kinematics and halo modeling. This agreement implies no significant unaccounted dark matter between the MW and M31, supporting the view that their halos dominate the LG's mass budget. Further refinements to the TA, integrating improved kinematics and cosmological simulations, are explored in Li & White (2008).

For the M81–M82 system, the symmetric mass distribution—with comparable contributions from major and minor components—yields a TA+simulation mass estimate of $M = 1.60^{+2.86}_{-1.07} \times 10^{12}\,M_\odot$. This aligns with virial and Hubble flow estimates, suggesting a relaxed dynamical state and reduced methodological tensions. The smaller uncertainties indicate that M81–M82 provides a simpler, more constrained system for dynamical studies. Despite being two nearby spiral galaxies consistent with TA mass estimates, we conclude they are likely on their first approach, as assumed by the TA framework.

In contrast, the Cen A–M83 system strongly favors the Projected CoM model, yielding a TA-derived mass of $1.48^{+0.68}_{-0.58} \times 10^{13}\,M_\odot$. While consistent with virial estimates, this value exceeds Hubble flow-based masses. The discrepancy arises from differing assumptions: TA and virial methods assume a bound system, whereas Hubble flow estimates may underestimate mass if unbound components contribute to large-scale dynamics.

Accurate proper motion measurements will enhance mass estimates for Cen A–M83. These data would constrain tangential velocities, reducing scatter in TA+simulation inferences and enabling a more complete dynamical framework. A full TA analysis incorporating tangential motion could surpass the current radial velocity-only approach, which inherently carries greater uncertainty. An alternative strategy involves leveraging dwarf galaxy kinematics, as demonstrated for M31 van der Marel & Guhathakurta (2008), or stellar tracers Salomon et al. (2021). Such methods may provide secondary kinematic constraints for Cen A–M83, though detailed analysis of satellite orbits will be reserved for future work.

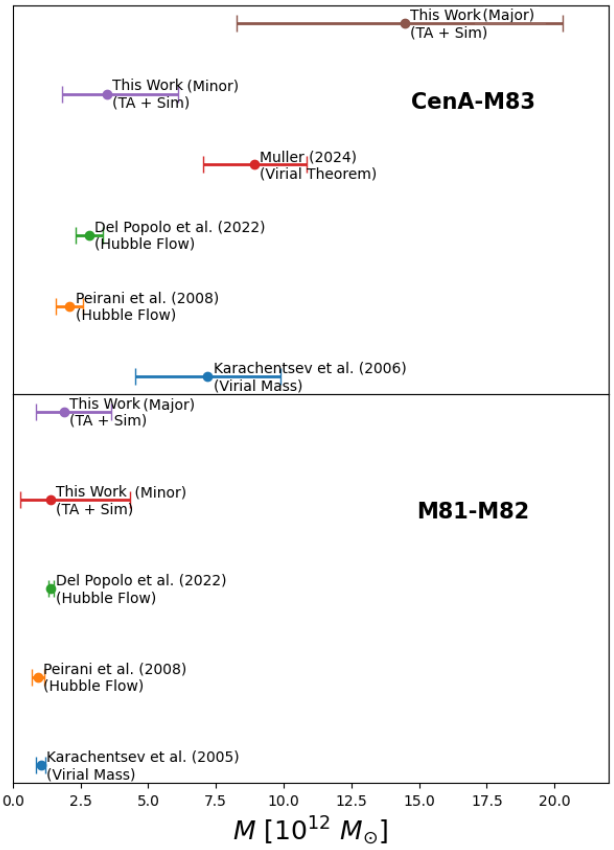

Fig. 8. *Comparison of mass estimates for two nearby galaxy systems, Cen A-M83 and M81-M82. The plots show the measured total mass using different methods: Virial Mass, Hubble Flow, and the TA.*

Acknowledgements. We thank Marcel Pawlowski and Jenny Wagner for useful discussions. DB is supported by a Minerva Fellowship of the Minerva Stiftung Gesellschaft fuer die Forschung mbH and acknowledges the contribution of the COST Actions CA23130 and CA21136. NIL acknowledges funding from the European Union Horizon Europe research and innovation program (EXCOSM, grant No.101159513). YH is partially supported by the Israel Science Foundation (ISF 1450/24).

References

Aghanim, N. et al. 2020, Astron. Astrophys., 641, A6, [Erratum: Astron.Astrophys. 652, C4 (2021)]
Allison, J. R., Sadler, E. M., & Meekin, A. M. 2014, MNRAS, 440, 696
Benisty, D. 2024, Astron. Astrophys., 689, L1
Benisty, D. & Capozziello, S. 2023, Phys. Dark Univ., 39, 101175
Benisty, D., Chaichian, M. M., & Tureanu, A. 2024 [arXiv:2405.14944]
Benisty, D. & Davis, A.-C. 2022, Phys. Rev. D, 105, 024052
Benisty, D., Vasiliev, E., Evans, N. W., et al. 2022, Astrophys. J. Lett., 928, L5
Chamberlain, K., Price-Whelan, A. M., Besla, G., et al. 2023, Astrophys. J., 942, 18
Courteau, S. et al. 2014, Rev. Mod. Phys., 86, 47
Damour, T. & Deruelle, N. 1985, Annales de l'I.H.P. Physique théorique, 43, 107
Del Popolo, A. & Chan, M. H. 2022, Astrophys. J., 926, 156
Diaz, J. D., Koposov, S. E., Irwin, M., Belokurov, V., & Evans, N. W. 2014, Mon. Not. Roy. Astron. Soc., 443, 1688
Díaz, R. J., Dottori, H., Aguero, M. P., et al. 2006, ApJ, 652, 1122
Gendre, M. A., Best, P. N., Wall, J. V., & Ker, L. M. 2013, MNRAS, 430, 3086
Hartl, O. V. & Strigari, L. E. 2022, Mon. Not. Roy. Astron. Soc., 511, 6193
Hartl, O. V. & Strigari, L. E. 2024 [arXiv:2411.07370]
Hunt, L. R., Johnson, M. C., Cigan, P. J., Gordon, D., & Spitzak, J. 2021, AJ, 162, 121
Jerjen, H., Freeman, K. C., & Binggeli, B. 2000, Astron. J., 119, 166
Karachentsev, I. D. 2005, Astron. J., 129, 178
Karachentsev, I. D. & Kashibadze, O. G. 2005 [arXiv:astro-ph/0509207]
Karachentsev, I. D. & Kashibadze, O. G. 2006, Astrophysics, 49, 3
Karachentsev, I. D. & Nasonova, O. G. 2010, Mon. Not. Roy. Astron. Soc., 405, 1075
Karachentsev, I. D., Sharina, M. E., Dolphin, A. E., et al. 2002, A&A, 385, 21
Karachentsev, I. D. et al. 2002, Astron. Astrophys., 389, 812
Karachentsev, I. D. et al. 2007, Astron. J., 133, 504
Karachentsev, I. D., Dolphin, A. E., Geisler, D., et al. 2002, A&A, 383, 125
Lemos, P., Jeffrey, N., Whiteway, L., et al. 2021, Phys. Rev. D, 103, 023009
Li, Y.-S. & White, S. D. M. 2008, Mon. Not. Roy. Astron. Soc., 384, 1459
Maksimova, N. A., Garrison, L. H., Eisenstein, D. J., et al. 2021, Mon. Not. Roy. Astron. Soc., 508, 4017
McLeod, M. & Lahav, O. 2020, JCAP, 09, 056
McLeod, M., Libeskind, N., Lahav, O., & Hoffman, Y. 2017, JCAP, 12, 034
Mo, H., van den Bosch, F. C., & White, S. 2010, Galaxy Formation and Evolution (Cambridge University Press)
Müller, O., Pawlowski, M. S., Lelli, F., et al. 2021, Astron. Astrophys., 645, L5
Müller, O., Pawlowski, M. S., Revaz, Y., et al. 2024, A&A, 684, L6
"Müller, O., Rejkuba, M., Fahrion, K., et al. "2024", To be published
Müller, O., Rejkuba, M., Pawlowski, M. S., et al. 2019, A&A, 629, A18
Partridge, C., Lahav, O., & Hoffman, Y. 2013, Mon. Not. Roy. Astron. Soc., 436, 45
Paturel, G., Petit, C., Prugniel, P., & Garnier, R. 1999, VizieR Online Data Catalog: Galaxy coordinates. II (Paturel, 1999), VizieR On-line Data Catalog: J/A+AS/140/89. Originally published in: 1999A&AS..140...89P
Peñarrubia, J., Gómez, F. A., Besla, G., Erkal, D., & Ma, Y.-Z. 2016, Mon. Not. Roy. Astron. Soc., 456, L54
Peñarrubia, J., Ma, Y.-Z., Walker, M. G., & McConnachie, A. 2014, Mon. Not. Roy. Astron. Soc., 443, 2204
Peirani, S. & de Freitas Pacheco, J. A. 2006, New Astron., 11, 325
Peirani, S. & Pacheco, J. A. D. F. 2008, Astron. Astrophys., 488, 845
Salomon, J. B., Ibata, R., Reylé, C., et al. 2021, MNRAS, 507, 2592
Sawala, T., Peñarrubia, J., Liao, S., & Johansson, P. H. 2023a, Mon. Not. Roy. Astron. Soc., 526, L77
Sawala, T., Teeriaho, M., & Johansson, P. H. 2023b, Mon. Not. Roy. Astron. Soc., 521, 4863
Speights, J. C. & Westpfahl, D. J. 2012, ApJ, 752, 52
Teerikorpi, P., Chernin, A. D., Karachentsev, I. D., & Valtonen, M. J. 2008, A&A, 483, 383
Truebenbach, A. E. & Darling, J. 2017, ApJS, 233, 3
Tully, R. B. et al. 2023, Astrophys. J., 944, 94
van der Marel, R. P., Fardal, M., Besla, G., et al. 2012, Astrophys. J., 753, 8
van der Marel, R. P. & Guhathakurta, P. 2008, Astrophys. J., 678, 187
van der Tak, F. F. S., Aalto, S., & Meijerink, R. 2008, A&A, 477, L5
Wagner, J. & Benisty, D. 2025 [arXiv:2501.13149]
Wang, W., Han, J., Cautun, M., Li, Z., & Ishigaki, M. N. 2020, Sci. China Phys. Mech. Astron., 63, 109801
Wempe, E., Lavaux, G., White, S. D. M., et al. 2024, Astron. Astrophys., 691, A348
Will, C. M. 2016, Gravity: Newtonian, Post-Newtonian, and General Relativistic, ed. R. Peron, M. Colpi, V. Gorini, & U. Moschella, 9–72

Appendix A: Mathematical Derivations and Vector Relations

This appendix provides a detailed overview of the vector relations used for the infall models. In the following, the equations are presented along with their respective interpretations and context. The unit vector $\hat{\boldsymbol{r}}_{21}$ is defined as the normalized vector pointing from $\boldsymbol{r}_1$ to $\boldsymbol{r}_2$. It is expressed as:

$$\hat{\boldsymbol{r}}_{21} = \frac{\boldsymbol{r}_2 - \boldsymbol{r}_1}{r_{21}} = \overline{r}_2 \hat{\boldsymbol{r}}_2 - \overline{r}_1 \hat{\boldsymbol{r}}_1 \ . \tag{A.1}$$

The orthogonality of $\hat{\boldsymbol{r}}_i$ and $\hat{\boldsymbol{r}}_{\perp i}$ for $i = 1, 2$ is given by:

$$\hat{\boldsymbol{r}}_i \cdot \hat{\boldsymbol{r}}_{\perp i} = 0 \ , \quad i = 1, 2 \ . \tag{A.2}$$

The cosine of the angle θ between the vectors $\hat{\boldsymbol{r}}_1$ and $\hat{\boldsymbol{r}}_2$ (and similarly between $\hat{\boldsymbol{r}}_{\perp 1}$ and $\hat{\boldsymbol{r}}_{\perp 2}$) is given by:

$$\hat{\boldsymbol{r}}_1 \cdot \hat{\boldsymbol{r}}_2 = \hat{\boldsymbol{r}}_{\perp 1} \cdot \hat{\boldsymbol{r}}_{\perp 2} = \cos\theta \ . \tag{A.3}$$

The sine of the angle θ between the vectors is expressed as:

$$\hat{\boldsymbol{r}}_1 \cdot \hat{\boldsymbol{r}}_{\perp 2} = -\hat{\boldsymbol{r}}_2 \cdot \hat{\boldsymbol{r}}_{\perp 1} = \sin\theta \ . \tag{A.4}$$

Next, the projections of $\hat{\boldsymbol{r}}_{21}$ onto the directions of $\hat{\boldsymbol{r}}_1$ and $\hat{\boldsymbol{r}}_2$ are as follows:

$$\hat{\boldsymbol{r}}_1 \cdot \hat{\boldsymbol{r}}_{21} = \overline{r}_2 \cos\theta - \overline{r}_1 \ , \quad \hat{\boldsymbol{r}}_2 \cdot \hat{\boldsymbol{r}}_{21} = \overline{r}_2 - \overline{r}_1 \cos\theta \ . \tag{A.5}$$

The projections of $\hat{\boldsymbol{r}}_{21}$ onto the perpendicular directions $\hat{\boldsymbol{r}}_{\perp 1}$ and $\hat{\boldsymbol{r}}_{\perp 2}$ are given by:

$$\hat{\boldsymbol{r}}_{\perp 1} \cdot \hat{\boldsymbol{r}}_{21} = -\overline{r}_2 \sin\theta \ , \quad \hat{\boldsymbol{r}}_{\perp 2} \cdot \hat{\boldsymbol{r}}_{21} = -\overline{r}_1 \sin\theta \ . \tag{A.6}$$

These equations provide the necessary mathematical framework to analyze vector relations in the context of the system described in the main text.